Vibration characteristics of the capillary in ultrasonic wire bonders

C M Hu[1], **N Q Guo**[1*], **H J Du**[1], **R M Lin**[1], and **M Chen**[2]
[1]School of Mechanical and Aerospace Engineering, Nanyang Technological University, Singapore
[2]Department of Control Science and Engineering, Nanjing Normal University, Nanjing, People's Republic of China

The manuscript was received on 15 December 2005 and was accepted after revision for publication on 4 September 2006.

DOI: 10.1243/09544062JMES265

Abstract: Currently ultrasonic wire bonders with precision capillary tips are widely used in the packaging industry for bonding wires to ICs and circuits. However, the quality and strength of a bond are affected significantly by the vibration of the bonding capillary. It is, therefore, necessary to study the vibration characteristics of the capillary for better understanding and for developing a non-perturbative and low-cost monitoring device for improving bonding quality control. In this paper, the vibration characteristics of the capillary are presented in terms of natural frequency and vibration modes using finite-element models. The predicted displacement profile along the capillary is compared with the measurement using a non-contact laser interferometer. In general, a good agreement between the prediction and measurement is obtained, and it shows that the interferometer may be a good monitoring tool for characterization of capillary tip vibration, as well as providing a reference for other monitoring devices.

Keywords: wire bonding, vibration of the capillary

1 INTRODUCTION

Wire bonders are the most important technology and machinery in the electronic packaging industry for connecting the silicon chip to the circuit board or the lead frame, which is a thin layer of metal that connects the wiring from tiny electrical terminals on the semiconductor surface to the large-scale circuitry on electrical devices and circuit boards. A gold or alumina wire is being driven by the ultrasonic vibration energy from the transducer assembly and being softened with the help of an electric spike to form a ball onto the pad [**1**]. The major components of the transducer assembly in the wire bonder is illustrated in Fig. 1, and they include a sandwiched piezoelectric composite transducer (A), which drives the longitudinal motion in the horizontal direction, a clamp or coupler (B), which is located on a node point and held by the bonding machine, a horn with a tapered profile (C), which amplifies the motion for a few times, and finally a capillary (D) which moves the wire and contacts with the pad. There are a couple of complex interconnections in the system as well, for example, the horn is mounted through a coupler or holder to the machine base, and the capillary is clamped on the tip end of the horn, and will be in direct contact with the lead frame during the bonding process. The electronic packaging industry is driving wire-bonding technology towards increased yields, decreased pitch and lowest possible cost [**1**, **2**]. Many new specific techniques and material issues are being developed and involved in achieving these goals, for example, decreased pitch requires a much higher frequency actuation, and a smaller size of the capillary.

Recently research and development efforts have been made to develop various numerical models for better understanding of the transducer components and the wire bonder assembly, and for design and optimization of wire bonders [**3–7**]. The multilayer piezoelectric transducer was studied numerically and experimentally [**3**, **4**, **8**], and the sensitivity of the parameters of the horn and their effects on the performance of the transducer were studied [**5**].

Corresponding author: School of Mechanical and Aerospace Engineering, Nanyang Technological University, 50 Nanyang Avenue, Singapore 639798, Singapore. email: mnqguo@ntu.edu.sg

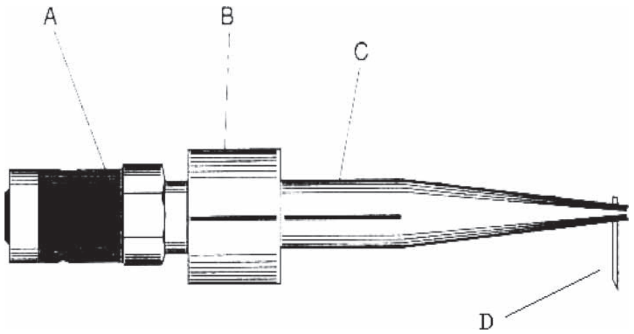

Fig. 1 Illustration of piezoelectric transducers used in ultrasonic wire bonders (A: transducer, B: clamp, C: horn, D: capillary)

Due to the multiple components in the wire bonder assembly, the interconnection of the components and their characteristics are very complex, for example, that between the horn of the transducer and the mounting holder, and that between the capillary and the lead frame. The contact characteristics of the horn-holder have recently been studied by a finite-element contact model, and the most significant design parameters are identified for the holder to minimize stress concentration and non-uniformity at the horn nodal cross-section [**5**]. Microslip phenomena has long been used to explain the mechanism of the contact between the capillary and the lead frame [**9**], and recently a quantitative microslip model has been developed to characterize the transient and steady state responses [**6**, **7**]. Attempt has been made to develop an integrated model in order to optimize the design and development of the transducer and wire bonder assembly [**10**], in which the characteristics of all the components in the wire bonders are coupled and their interaction and impact on the design and optimization are discussed.

However, among the components in the wire bonder the capillary has received less attention. As a bonding tool, the capillary is to bring the materials being bonded to contact under an external static compressive force pressed on the top of the capillary, producing some initial deformation but no adhesion due to the presence of surface film or oxides. Driven by longitudinal vibration of the ultrasonic transducer in the horizontal direction, the capillary oscillates in the transverse direction and results in an oscillatory force parallel to the wire–pad interface. Thus, the wire softens upon absorption of ultrasonic energy and flows under loading, breaking up the surface oxides, and exposing a fresh surface of both the wire and the bonding pad. These freshly exposed surfaces of metal cold-weld readily. The interfacial movement is progressively restricted by the formation of multiple micro-welds in the peripheral area of the contact zone. Continued application of cyclic stresses produces plastic deformation of the wire, increasing the contact area, and resulting in weld area, under the effect of the static force [**9**].

The optimization of capillary design configuration is one of the most critical parameters that influence the final bonding quality as evidenced by the test done by the manufacturers [**2**], in which a capillary response test was carried out using a laser interferometer. The oscillation test study was conducted to determine if there is any difference in the amplitude response between different materials. It is essential to understand the vibration of the capillary as it is the only coupling component of the transducer and bonding pad during the bonding process. It is also desirable in the packaging industry to develop a monitoring device to measure the variation of the vibration characteristics, which are directly related to the quality of the bond. The current paper presents the vibration modelling of the capillary used in wire bonders, and a comparison with measurement using a laser interferometer, and finally the discussion on the effective boundary condition of the capillary, which is mounted on the transducer horn.

2 ANALYSIS

In this section, the free vibration characteristics such as natural frequency and mode shape of the capillary were first obtained with finite-element analysis, followed by the forced vibration response where the capillary is driven by the transducer. The dimensions of the capillary may vary according to different designs and different manufacturers as shown in the capillary catalogues [**11**, **12**]. In this work, the capillary (Series # 41413-0010-320) from Micro-Swiss [**12**] was used in the K&S wire bonder [**13**], and hence its characteristics were used in modelling. According to the catalogue, the capillary is designed to provide an optimum performance on automatic wire bonders with the following features.

1. A 120° inner chamfer angle which grips and centres the ball during the first bond, producing a bell-shaped bond with low ball deformation.
2. A larger tip diameter with a big effective face, which allows more contact with wire during the stitch bond, resulting in a stronger wedge-shaped bond which is less likely to lift.
3. A large face angle (FA) that provides a larger second bond cross-section, resulting in a stronger bond. The FA and core apex is sharp for consistent cutoff, and blends into a larger outer radius for smooth transition of the bond into the wire.

The dimensions of the capillary model are illustrated in Fig. 2 with a wire diameter of 25 μm to be used. The

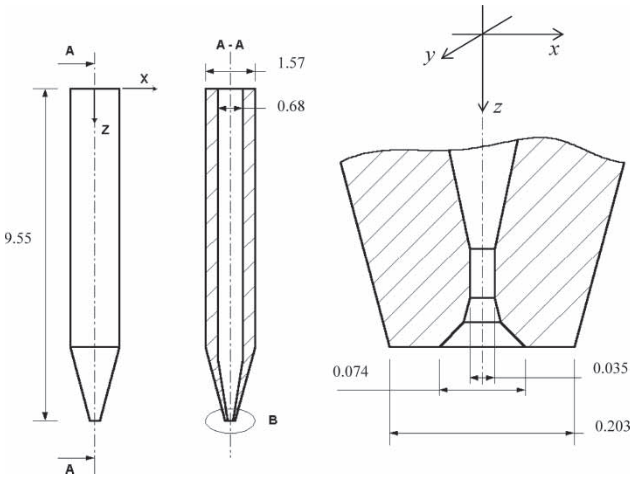

Fig. 2 Dimensions (mm) and directions of the capillary used in this study: (a) capillary and its defined directions and (b) enlarged view of the tip B

total length of the capillary is 9.55 mm and the tip of the capillary is polished and has a 30° cone. The capillary is made of Alumina (Al_2O_3), and its material properties used in the finite-element model are of density 3960 kg/m^3, Young's modulus of 379 GPa, and Poisson's ratio of 0.22 [**14**]. A solid three-dimensional element is used in simulation, which is a brick element, defined by eight nodes with three degrees-of-freedom (DOF) at each node: translation in the nodal x-, y-, and z-directions [**15**].

Modal analysis was first performed on the capillary model to obtain its natural frequencies and corresponding mode shapes. Forced vibration was then performed using the harmonic response analysis on the model, assuming constant transverse displacement load on the root portion of the capillary, which is proven by the experiment in the following section. The amplitude response was also calculated in the frequency range from 0 to 400 kHz. The meshed model of the capillary is shown in Fig. 3 for the modal analysis, and the boundary condition was set by constraining all the nodal DOF at the top of the capillary as illustrated in Fig. 3(b) corresponding to the clamping condition that the capillary is mounted to the transducer horn by the bolts. The longitudinal direction in the capillary model is set along the z-axis (i.e. along the length of the capillary) whereas x- and y-axis are the transverse direction (i.e. horizontal direction), and the x-direction being the vibrating direction of the horn, as defined in Fig. 2. Resonance modes are obtained in the frequency range of interest (0–300 kHz), their natural frequency and types of mode shapes are listed and identified in Table 1, and the mode shapes of the transverse modes within the range are shown in Fig. 4.

It can be seen that the first mode at 33 kHz is the first-order transverse mode in the x-direction as shown in Fig. 4(a), which shows a simple bending motion with maximum amplitude at the free end. A double mode at the same frequency with transverse motion in the y-direction was also predicted due to axial symmetry about the z-axis. However, only the vibration in the x-direction is to be excited by the transducer due to the force exerted by the transducer horn being along the x-direction. The third mode at 179 kHz is the second-order transverse mode in the x-direction as shown in Fig. 4(b), followed by another double mode in the y-direction at same frequency. A nodal point is expected along the length of the capillary in the second-order transverse modes where the transverse displacements are zero. However, the modes are far above the exciting frequency of the transducer at 60 kHz in the current 60 kHz wire bonders, they have little influence within the frequency range of interest in the forced vibration response.

The fifth mode at 204 kHz is the first-order torsional mode of the capillary. Since the exciting force by the transducer horn is applied in the x-direction, the torsional mode cannot be excited, and will not appear in the forced vibration response. The last mode within

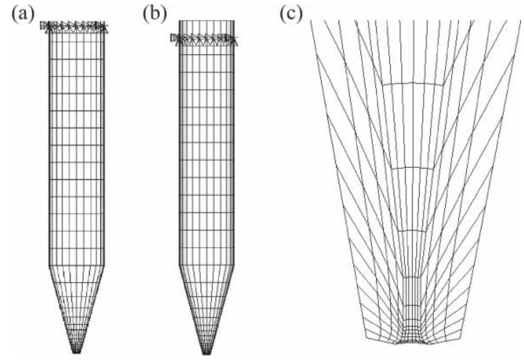

Fig. 3 Meshed models of the capillary used for the finite-element modal analysis: (a) the meshed elements of the capillary; (b) with different boundary condition; and (c) the meshed detail at the tip

Table 1 Predicted natural frequencies and the vibration modes of the capillary

Number	Natural frequency (kHz)	Vibration mode
1	32.979	First-order transverse in the x-direction
2	32.979	Double mode in the y-direction
3	178.86	Second-order transverse in x-direction
4	178.86	Double mode in the y-direction
5	204.01	First-order torsional mode
6	285.11	First-order extensional mode

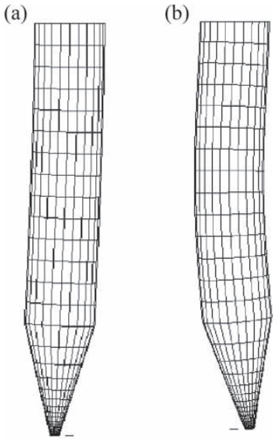

Fig. 4 Predicted transverse mode shape of the capillary using finite element analysis: (a) first transverse mode at 33 kHz and (b) Second transverse mode at 179 kHz

the 300 kHz range is the first-order extensional mode at 285 kHz, and the mode vibrates in the longitudinal direction (z), i.e. along the length direction of the capillary. Similar to the torsional mode, the extensional mode will not be excited by the applied force from the transducer horn, which is in the horizontal direction.

The undamped harmonic response analysis was then obtained as a function of frequency, and a constant displacement load of varying frequency in the x-direction was applied across the root of the capillary to simulate the load being applied by the vibration of the horn in the horizontal direction. This is a valid approximation since the vibration study on the transducer–horn assembly showed that the end of the horn exhibits an almost uniform longitudinal vibration in the horizontal direction [**10**]. Figure 5 shows the predicted frequency response function of the capillary tip in the transverse direction (the x-direction) from 1–400 kHz, with resonance peaks at 33 and 179 kHz, respectively. It can be seen clearly that only the first

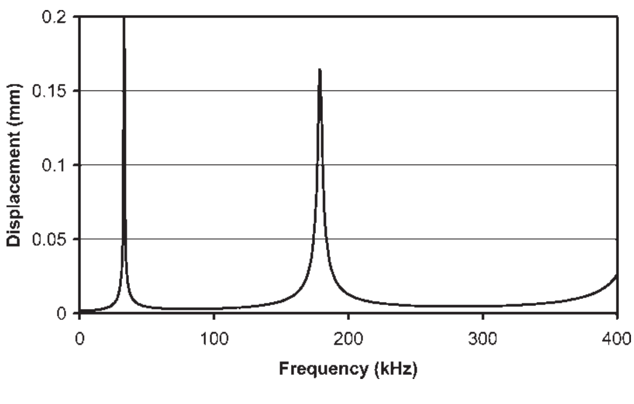

Fig. 5 Predicted frequency response function at the tip of the capillary where the first and second transverse modes can be excited

and second transverse modes of the capillary can be excited, and the torsional and extensional modes of the capillary cannot be excited by the forcing condition as mentioned before. It is noted that when the wire bonder is operating at the nominal frequency of 60 kHz, the capillary is not driven at its resonance frequency, and the vibration profile at the driving frequency will have contributions from both the first and second resonance modes.

3 MEASUREMENT OF THE CAPILLARY VIBRATION

Since the capillary is driven at 60 kHz by the transducer through the horn, the vibration profile of the capillary at the driving frequency was measured and is discussed in this section. The vibration profile is defined as the transverse amplitude, a function of the capillary length, starting from the root at 0 mm (where the capillary is clamped to the horn) to the free tip at 9.55 mm (where the gold ball is bonded onto the die) (Fig. 2). The predicted displacement profile with different boundary conditions is calculated and compared with the measured one. Then the correct boundary condition, which is already used in the previous section, is discussed.

The vibration of the capillary free from loading (without wire) was measured using a laser scanning vibrometer (Polytec PSV300). It is a laser vibrometer that uses an interferometer technique to measure vibration. The light source of the vibrometer is a helium neon laser. Optical interferometer allows the measurement of vibration much smaller than the wavelength of light by utilizing the sinusoidal relationship between the output of an interferometer and the difference in optical path lengths traversed by its beam. Figure 6 shows an enlarged picture of the capillary clamped on the horn of the transducer with a side screw. This picture was captured using a video camera in the scanning head of PSV300, and the mesh points represent the positions at which the laser interferometer would scan and measure automatically. The direction of the velocity measured is parallel to the horn direction, i.e. transverse direction to the capillary axis.

The measured result shown in Fig. 7 is the fast Fourier transform (FFT) spectrum of the measured velocity signal. It can be seen that the steady state forced vibration is dominated by the exciting frequency at 60 kHz. However, there are other resonant peaks appearing in the signal, at 180, 240 and 310 kHz, respectively. There are harmonic components in the force signal due to non-linearity property. The resonant peak at 180 kHz can be identified as the second transverse mode predicted at 179 kHz, and it could be excited by the third harmonic component of the

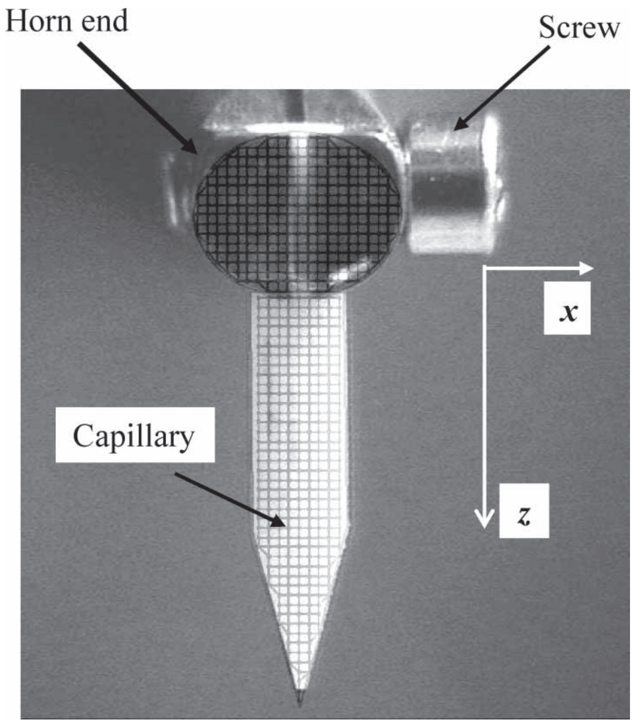

Fig. 6 Captured picture of the capillary showing the mesh of the measured points by the interferometer

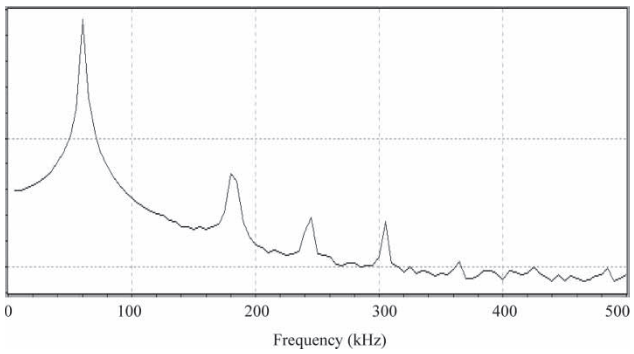

Fig. 7 FFT spectrum of the measured velocity signal at the driving frequency of 60 kHz

driving frequency. However, it is unclear, what the other resonances appearing at 240 and 310 kHz are due to? Nevertheless, they are insignificant since the frequency range of interest is well below 200 kHz.

Since the prime interest is in the vibration characteristics at 60 kHz, only vibration amplitude and profile at the driving frequency of 60 kHz are discussed. Figure 8 shows the measured three-dimensional velocity profile along the capillary length from the clamping point at the horn to the capillary tip with driving frequency being 60 kHz, where the horizontal axes are the location coordinates, one being the length direction (z) and the other being the transverse direction (x) (Fig. 6), and the vertical axis is the velocity amplitude. It can

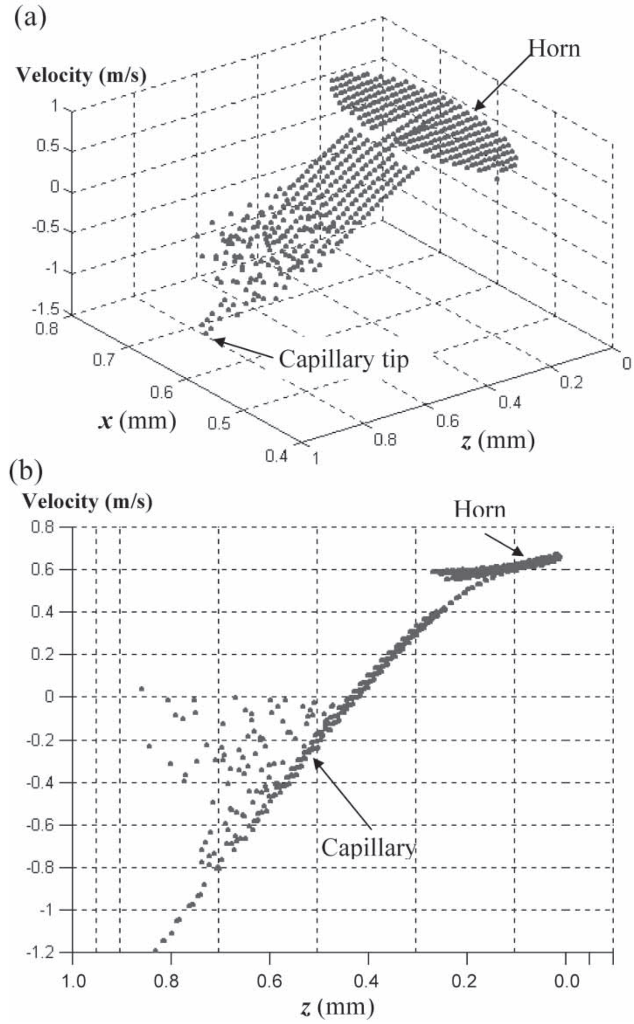

Fig. 8 Measured velocity profile of the capillary using the interferometer: (a) velocity versus measured plane and (b) side view along the length position

be seen that the whole surface of the horn tip moves in planar motion, and the capillary moves in a see-saw fashion with one nodal point in the middle at which the amplitude is zero. It can also be seen that the velocity amplitude of the capillary is a function of the longitudinal coordinate only (along the length of the capillary), and there is little variation of amplitude near the capillary root. This has justified the assumption used in the previous modal analysis that a uniform transverse displacement was applied to the root portion of the capillary. Some scatters are also seen at the locations near the capillary tip since the section is smaller and curved and the interferometer was not able to measure the vibration velocity accurately due to the scattering of the laser beam onto the curved section.

Figure 8(b) shows the velocity amplitude along the capillary length. It can be seen from Fig. 8(b) that the measured velocity reduces gradually along the length of the capillary with a nodal point about half way. The lower part of the capillary has velocity in the negative direction, increasing in amplitude and reaching a maximum at the tip of the capillary. It is hence evident that the velocity profile is different from the first mode shape of the cantilever beam, and this is likely due to the effective boundary condition that the capillary is loaded at its connecting point with the vibrating horn.

The effective boundary condition of the capillary should be determined carefully because it will influence the vibration characteristics of the capillary. Two boundary conditions were considered to refine the model used for simulation of the capillary vibration. One is shown in Fig. 3(a) where the nodes in the first line are fixed in the y- and z-direction, but they are allowed to move in the x-direction, which is driven by the horn vibration. The steady-state displacement loading amplitude is 1.778 μm that was obtained from the experiment at frequency of 60 kHz. The other case is shown in Fig. 3(b) where the nodes in the second line are pinned in the y- and z-direction, and they are allowed to oscillate at the driving frequency with amplitude of 1.699 μm in the x-direction.

The simulated vibration profiles with different boundary conditions and the measured result along the middle axis line of the capillary are plotted in Fig. 9. The measured displacements, shown as cross symbols, were obtained by dividing the measured velocity with the exciting angular frequency. The solid line is the predicted displacement profile with the first boundary condition, and the broken line is the profile predicted with the second case. It can be seen clearly that the predicted displacement profile with the first boundary condition has a better quantitative agreement with the measured one. The vibration profile resembles the first-order transverse mode with an offset that is due to the applied displacement loading by the vibrating horn, a nodal point can thus be observed at about 4.6 mm from the root of the capillary. The effective boundary condition would be used to couple both transducer horn and the capillary, and used in further modelling the wire bonder. It is expected that if the capillary is driven at a much higher frequency, for example, at 120 kHz, the influence and contribution of the second-order transverse mode would be more significant. To keep the simple vibration profile as observed, the dimensions of the capillary would have to be modified.

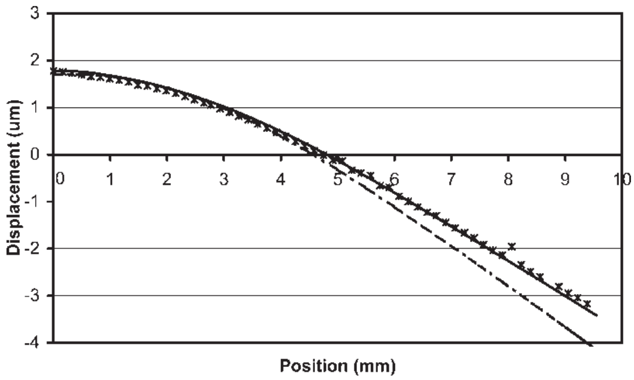

Fig. 9 Measured and predicted displacement profile of the capillary with different boundary conditions at the root (symbol: experiment; broken line: fixed at second line; and solid line: fixed at first line)

4 CONCLUSIONS

The vibration characteristics of a typical capillary used in the transducer of a wire bonder have been analysed using finite-element models. It can be seen that the first-order transverse resonance frequency of the capillary at 33 kHz is well within the operating frequency of 60 kHz. The capillary exhibits a second-order transverse resonant frequency at 179 kHz, which is much higher than the operating frequency, and hence has less influence on the vibration characteristics. However, with the development of fine pitch wire bonders, higher frequencies of 100–120 kHz transducer is to be used, the effect of this second-order transverse mode will have to be considered on the vibration pattern of the capillary. Appropriate capillary needs to be designed with the introduction of the high-pitch transducer. The predicted displacement profile at the operating frequency of 60 kHz has been verified with the experimental results, which were measured using a laser interferometer. It is found that there is a good quantitative agreement between prediction and measurement. It shows that the laser interferometer can provide a good non-contact measurement tool for characterization of vibration analysis of capillary, and can be used as a reference for measurement by other techniques due to its accuracy.

REFERENCES

1 **Harman, G.** *Wire bonding in microelectronics materials, processes, reliability, and yield*, 2nd edition, 1998 (McGraw-Hill, New York).
2 **Castaneda, J.** and **Bautista, W.** *Optimization of capillary configuration for a robust design*. Report of SPT Asia Pte. Ltd, 1997, pp. 133–143.
3 **Or, S. W., Chan, H. L. W., Lo, V. C.,** and **Yuen, C. W.** Dynamics of an ultrasonic transducer used for wire bonding. *IEEE Trans. Ultrason. Ferroelectr. Freq. Control*, 1998, **45**, 1453–1460.
4 **Kang, S. Y., Williams, P. M.,** and **Lee, Y. C.** Modeling and experimental studies on thermosonic flip-chip bonding. *IEEE Trans. Compon. Packag. Manuf. Technol. B*, 1995, **18**, 728–733.

5 **Jang, C., Ahn, G. S., Kim, Y. J., Kwak, D. O., Booh, S. W.,** and **Kim, J. O.** Finite element contact analysis on a horn-holder assembly for wire bonding. *IEEE Trans. Electron. Packag. Manuf.*, 2003, **26**(1), 46–53.
6 **Hu, C. M., Guo, N., Du, H., Li, W. H.,** and **Chen, M.** A microslip model of the bonding process in ultrasonic wire bonders. Part I: transient responses. *Int. J. Adv. Manuf. Technol.*, 2006, **29**(9–10), 860–866.
7 **Hu, C. M., Guo, N., Du, H.,** and **Jian, X. M.** A microslip model of the bonding process in ultrasonic wire bonders. Part II: steady state responses. *Int. J. Adv. Manuf. Technol.*, 2006, **29**(11–12), 1134–1142.
8 **Hu, C. M., Guo, N., Du, H.,** and **Xu, L. M.** Dynamic characteristics of stacked piezoelectric transducers of ultrasonic wire-bonders used in integrated circuit packaging. *Proc. Instn Mech. Engrs, Part C: J. Mechanical Engineering Science*, 2003, **217**, 341–352.
9 **Chen, G. K. C.** The role of micro-slip in ultrasonic bonding of microelectronic dimensions. International Hybrid Microelectronics Symposium, Vol. 20(5A), 1972, pp. 111–119.
10 **Hu, C. M., Guo, N., Du, H.,** and **Chen, M.** A coupled finite element model for ultrasonic wire bonders. *IEEE Trans. Electron. Packag. Manuf.*, submitted.
11 **SPT (Small Precision Tools).** *SPT user's manual, bonding capillaries*, 1997.
12 **Micro-Swiss.** *Micro-Swiss capillary catalogue*, 1999.
13 **Kulicke & Soffa.** *Kulicke & Soffa 4500 Series Manual – wire bonders operation and maintenance manual*, 1998.
14 **Kingery, W. D., Bowen, H. K.,** and **Uhlmann, D. R.** *Introduction to ceramics*, 2nd edition, 1975 (John Wiley & Sons, New York).
15 **Ansys.** *ANSYS user's manual, version 5.6*, 1999.